

Article

The Properties of Magnesium Silicate Hydrate Prepared from the Magnesium Silicate Minerals in the Earth's Crust

Qiang Song¹, Qian He¹, Jiao Nie¹, Tiantian Song¹, Hong Zhou², Yaru Hu¹, Yanxin Chen^{1,*}, Yang Deng³ and Fuan Cheng¹

¹ College of Materials Science and Engineering, Xi'an University of Architecture and Technology, Xi'an 710055, China; songqiang123@xauat.edu.cn (Q.S.); heqian@xauat.edu.cn (Q.H.); niejiao@xauat.edu.cn (J.N.); songtiantian@xauat.edu.cn (T.S.); huyaru@xauat.edu.cn (Y.H.); chengfuan@xauat.edu.cn (F.C.)

² Shaanxi Building Materials Technology Group Co., Ltd., Xi'an 710018, China; zh3524254219@163.com

³ Shaanxi Fuping Eco-Cement Co., Ltd., Weinan 711709, China; hunt7758ppty@163.com

* Correspondence: chenyanxin@xauat.edu.cn

Abstract: In order to explore a wider range and lower cost of raw materials for the preparation of magnesium silicate hydrate (M-S-H), an acid-leaching method was employed to extract and separate high-purity magnesium hydroxide ($\text{Mg}(\text{OH})_2$) with a purity higher than 97% and amorphous silica with a purity higher than 90% from four types of natural silicate minerals (serpentine, peridotite, zeolite, and montmorillonite). These two intermediate products, which are amorphous silica and magnesium hydroxide, were used to prepare M-S-H, and the influence of curing at two temperatures, 50 °C and 80 °C, on the properties of M-S-H was investigated. The results showed that with the increase in curing temperature, the bound water content, tetrahedral polymerization degree, and $\text{Mg}(\text{OH})_2$ content increased. There was a good correlation between the increase in strength and the bound water content of M-S-H. This work provides a possible technological route for expanding the raw materials for preparing magnesium silicate hydrate cementitious materials and utilizing the abundant magnesium silicate minerals in the Earth's crust.

Keywords: magnesium silicate minerals; magnesium silicate hydrate; acid-leaching method; strength



Citation: Song, Q.; He, Q.; Nie, J.; Song, T.; Zhou, H.; Hu, Y.; Chen, Y.; Deng, Y.; Cheng, F. The Properties of Magnesium Silicate Hydrate Prepared from the Magnesium Silicate Minerals in the Earth's Crust. *Buildings* **2024**, *14*, 1188. <https://doi.org/10.3390/buildings14051188>

Academic Editor: Shengwen Tang

Received: 5 March 2024

Revised: 8 April 2024

Accepted: 16 April 2024

Published: 23 April 2024



Copyright: © 2024 by the authors. Licensee MDPI, Basel, Switzerland. This article is an open access article distributed under the terms and conditions of the Creative Commons Attribution (CC BY) license (<https://creativecommons.org/licenses/by/4.0/>).

1. Introduction

Hydrated magnesium silicate (M-S-H) cementitious material is considered to be a low-carbon cementitious material [1] and is typically prepared by reaction of MgO or $\text{Mg}(\text{OH})_2$ with amorphous, reactive silica in the presence of water [2]. $\text{Mg}(\text{OH})_2$ and MgO are usually obtained from carbonate rocks such as magnesite and dolomite or Mg^{2+} in salt lakes and seawater. These methods result in direct or indirect CO_2 emissions. Silica fume is the most common source of Si in the solution reaction method for preparing M-S-H [3–6]. In addition, amorphous SiO_2 present in rice husk ash [7], fly ash [8], fluidized bed bottom ash [9], finely ground waste glass, and diatomaceous earth [10] can also serve as reactants for the formation of M-S-H. Amorphous SiO_2 and silicic acid [11,12] exhibit higher reactivity compared to crystalline SiO_2 . As a supplementary cementitious material, the high cost and specific locality of silica fume limit its use as a cementitious material.

The molar ratio of magnesium to calcium (Mg:Ca) in the continental crust is approximately 1.06, as reported by Hans [13]. This brings to light an intriguing question: is it feasible to utilize naturally occurring magnesium silicate minerals for the synthesis of hydrated magnesium silicate cementitious materials? The potential use of natural magnesium silicate minerals as raw materials in the production of such cementitious materials offers a dual advantage. First, it presents an opportunity to significantly reduce carbon dioxide emissions, as this process circumvents the need for calcining magnesium carbonate.

Second, it proposes a cost-effective route for manufacturing hydrated magnesium silicate, thus making it an attractive alternative to traditional cementitious materials.

Ruiter's research delineates the serpentinization process of olivine-rich rocks, which leads to the formation of brucite. This brucite subsequently dissolves, yielding a magnesium-rich fluid with a notably high pH level (exceeding 9). This alkaline fluid facilitates the dissolution of quartz, culminating in the emergence of a nanocrystalline magnesium silicate hydrate phase [14]. Among magnesium silicate rocks such as serpentine, olivine, sepiolite, and chlorite, there is a notable absence of cementing properties. But, after undergoing dehydration, natural serpentine demonstrates commendable cementitious qualities upon rehydration within autoclave conditions, achieving a compressive strength of up to 17 Mpa [15]. Furthermore, within acidic environments, the trio of minerals—serpentinite, leaf serpentinite, and fiber serpentinite—are capable of dissolving Mg^{2+} and amorphous SiO_2 . The purpose of this study is to use natural magnesium silicate minerals as raw materials to prepare hydrated magnesium silicate gelling materials. The characteristics of the magnesium silicate hydrate (M-S-H) derived from isolated $Mg(OH)_2$ and amorphous SiO_2 were meticulously analyzed through the dissolution of serpentine, peridotite, sepiolite, and chlorite in sulfuric acid. It provides a new path for preparing hydrated magnesium silicate cementing materials.

2. Materials and Methods

2.1. Materials

Serpentine, peridotite, sepiolite, and chlorite are derived from Shanlin Shiyu Mineral Products Co., Ltd., Guzhang County, Xiangxi Prefecture, Hunan Province. The chemical composition is shown in Table 1, the X-ray diffraction is shown in Figure 1, and the particle size distribution of the raw materials is shown in Figure 2. Serpentine consists mainly of serpentine group minerals such as Elisserite, fibrous serpentine and leaf serpentine, and plagioclhorite and contains a small amount of magnetite. Peridotite is mainly composed of magnesium olivine. Chlorite is mainly composed of plagioclhorite and brittle chlorite. The silica and magnesium contents of the four minerals are high, which provide rich silicon and magnesium sources for the preparation of hydrated magnesium silicate cementing materials. The particle size distribution analysis of raw materials (as shown in Figure 2) indicates that the mean particle size of serpentine, olivine, sepiolite, and chlorite is 70 μm , 80 μm , 80 μm , and 70 μm , respectively.

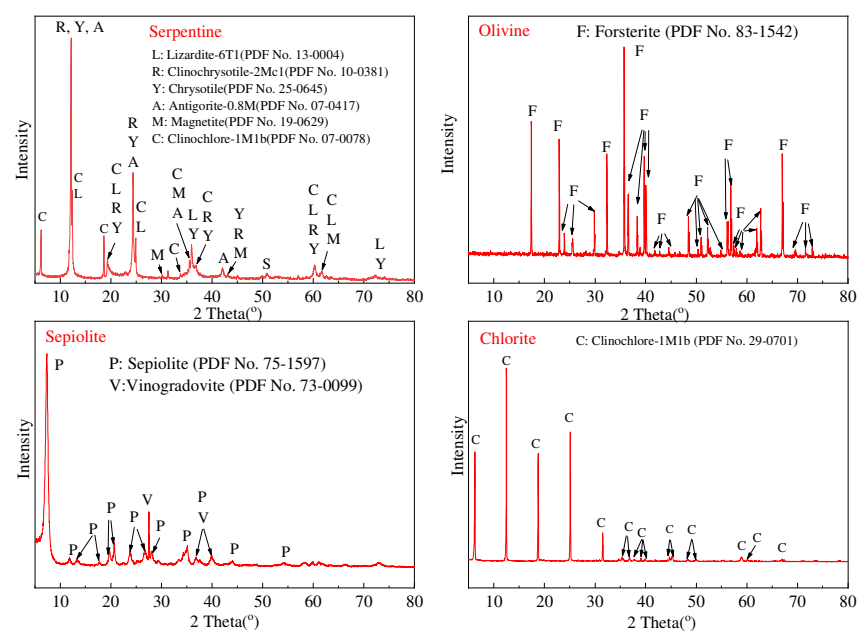
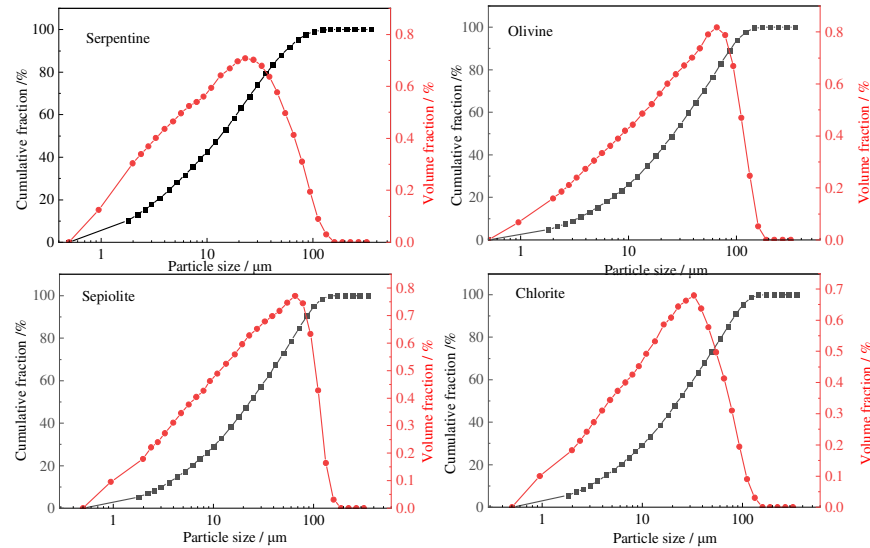


Figure 1. XRD of raw materials.

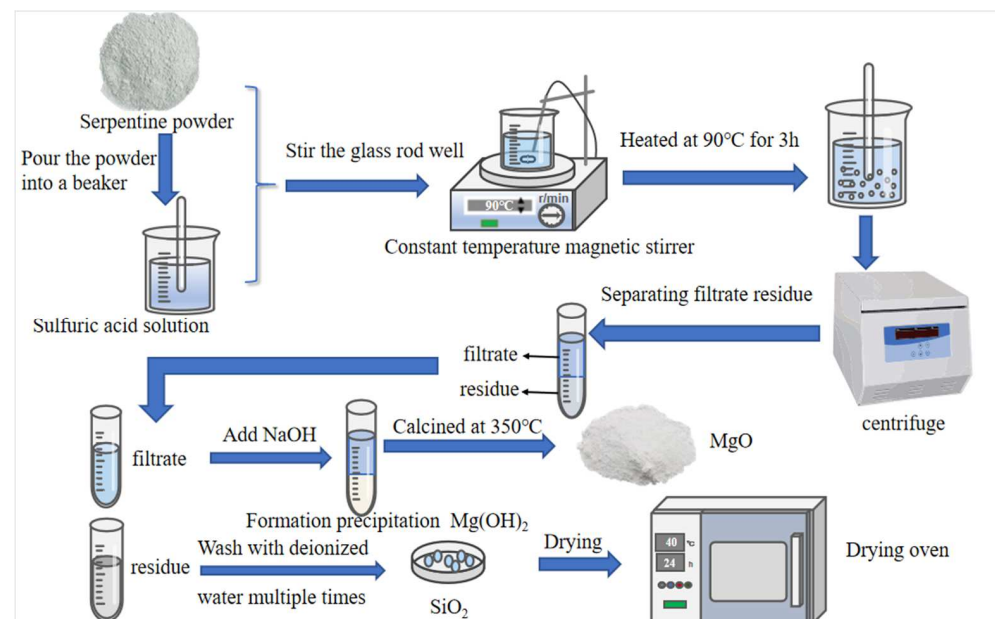
Table 1. Chemical composition of raw material wt%.

Materials	MgO	SiO ₂	Al ₂ O ₃	Fe ₂ O ₃	CaO	K ₂ O	Na ₂ O	TiO ₂
Serpentine	43.48	45.95	0.62	9.11	0.37	0.02	0.11	0.02
Olivine	47.89	41.77	0.23	9.97	0.08	0.01	0.04	0.01
Sepiolite	28.47	67.45	2.03	0.49	0.44	0.65	0.28	0.09
Chlorite	34.71	42.12	12.70	6.96	3.12	0.12	0.05	0.22

**Figure 2.** Particle size distribution of raw materials.

2.2. Methods

The schematic diagram of the experiment is shown in Figure 3. The raw materials (serpentine, olivine, sepiolite, and chlorite) were dissolved in a 30% H₂SO₄ solution with a solid–liquid ratio of 1:5 and heated at 90 °C for 3 h. After dissolution, the solution was separated from the residue using a centrifuge. The residue was washed five times with deionized water and then dried in an oven at 50 °C until a constant weight was reached. The dried residue was sealed and stored for later use.

**Figure 3.** A schematic diagram of the experiment.

To obtain precipitation, NaOH solution was added dropwise to the separated filtrate using a Pasteur pipette. The resulting precipitation was clarified, separated, and dried to obtain Mg(OH)₂. Since the newly formed Mg(OH)₂ is more conducive to the formation of M-S-H [16], in this experiment, Mg(OH)₂ was calcined to produce MgO, which served as the magnesium source for the preparation of M-S-H. The dried precipitated sample was calcined at 350 °C in a muffle furnace for 1 h, resulting in white MgO powder.

The resulting residue was then mixed evenly with MgO powder in a mass ratio of 6:4, and a paste was prepared using deionized water at a water-to-solid ratio of 1:2. After sealing, the paste was cured in a constant temperature water bath at 50 °C and 80 °C for 3 days, 7 days, 14 days, and 28 days, respectively. Subsequently, the cured samples were dried in a vacuum drying oven at 40 °C for 24 h.

The mineral phase analysis was undertaken using an XRD (D8, Bruker, Berlin, Germany) with CuK α radiation operating at 40 kV/30 mA and scanning the range from 5 to 80 at a speed of 3°/min. Particle size distribution (PSD) was determined by using a laser particle size analyzer. Thermogravimetric analysis (TGA) was performed by using a METTLER (Bern, Switzerland) Toledo TGA/DSC1/1600 thermal analysis system with a temperature accuracy of ± 0.5 °C. Fourier transform infrared (FTIR) spectra were obtained by using a spectrometer (Nicolet IS50, Thermo Fisher, Madison, WI, USA). The FTIR analysis had a resolution of 4 cm⁻¹ and co-addition of 32 scans. The magic-angle rotating solid high-resolution NMR experiments were carried out using an AVANCE400 (SB) fully digital NMR spectrometer of Bruker (Bern, Switzerland), and a solid 15 N~31 P probe of 4 mm/15 kHz.

The strength of the mortar samples was tested according to the GB/T 17671-1999 [17]. The mass ratio of the residue to MgO in the cementing material was 6:4, with 0.2% polycarboxylate superplasticizer. The water–cement ratio for the mortar samples was 0.5. The specimen size was 40 mm \times 40 mm \times 160 mm, and the specimens were cured in a water bath at 50 °C and 80 °C for the specific age to measure compressive strength.

3. Results and Discussion

3.1. Composition and Particle Size Distribution of the Residue and Mg(OH)₂

The chemical composition of the residue and Mg(OH)₂ are shown in Table 2. The XRD patterns of the residue, Mg(OH)₂ and MgO calcined, are shown in Figures 4 and 5. In Table 2, the chemical composition of the residue is mainly SiO₂, a minor of SO₃ introduced from sulfuric acid, and other components. The XRD pattern reveals diffraction peaks of amorphous SiO₂ in the range of $2\theta = 15^\circ$ to 30° , while no distinct crystal diffraction peaks are observed for residue dissolved from serpentine, olivine, and sepiolite.

Based on Figures 4 and 5 and Table 2, the obtained Mg(OH)₂ and the MgO derived from calcination at 350 °C exhibit relatively high purity. The particle size distribution analysis of the residue (amorphous silica) and Mg(OH)₂ precipitation (as shown in Figure 6) indicates that the mean particle size of the amorphous SiO₂ prepared from serpentine is approximately 20 μ m, while that from olivine and sepiolite is around 30 μ m. For chlorite, the mean particle size is approximately 65 μ m. Similarly, the maximum particle size of Mg(OH)₂ precipitated from the four types of minerals is approximately 65 μ m.

Table 2. Results of chemical analysis of residue and Mg(OH)₂ wt%.

Materials		SiO ₂	MgO	SO ₃	Al ₂ O ₃	Fe ₂ O ₃	CaO	K ₂ O	Na ₂ O	TiO ₂
Residue	Serpentine	94.68	0.78	3.97	0.09	0.34	0.06	0.01	0.05	0.02
	Olivine	95.74	1.35	1.33	0.25	0.92	0.16	0.02	0.08	0.15
	Sepiolite	95.69	1.72	1.45	0.65	0.20	0.15	/	/	0.14
	Chlorite	90.87	5.44	0.88	/	2.61	/	/	/	0.20
Mg(OH) ₂	Serpentine	0.52	98.22	0.52	0.06	0.64	/	/	0.04	/
	Olivine	2.03	96.82	0.32	0.21	0.19	0.12	0.01	0.30	0.01
	Sepiolite	0.38	98.69	0.05	0.60	/	0.08	/	0.20	/
	Chlorite	1.94	97.12	0.24	0.33	0.24	/	0.02	0.11	/

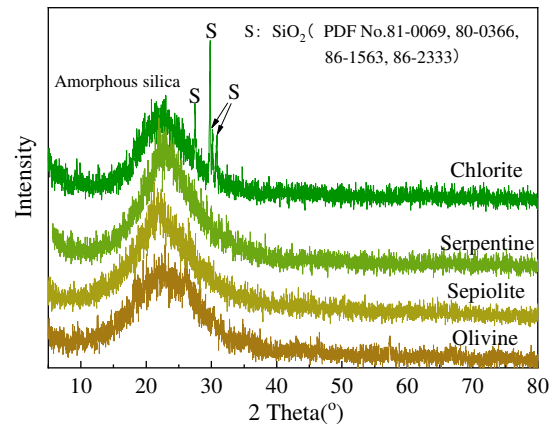


Figure 4. XRD of filter residue.

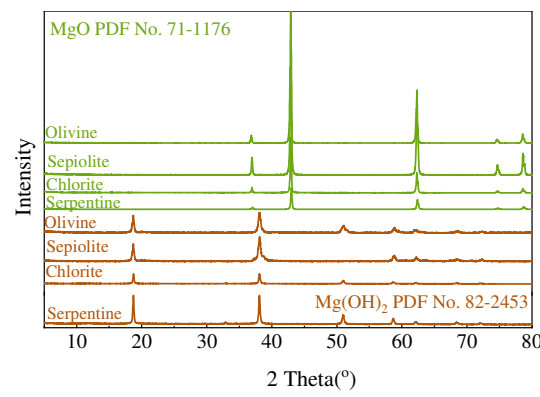


Figure 5. XRD of filter Mg(OH)₂ and MgO.

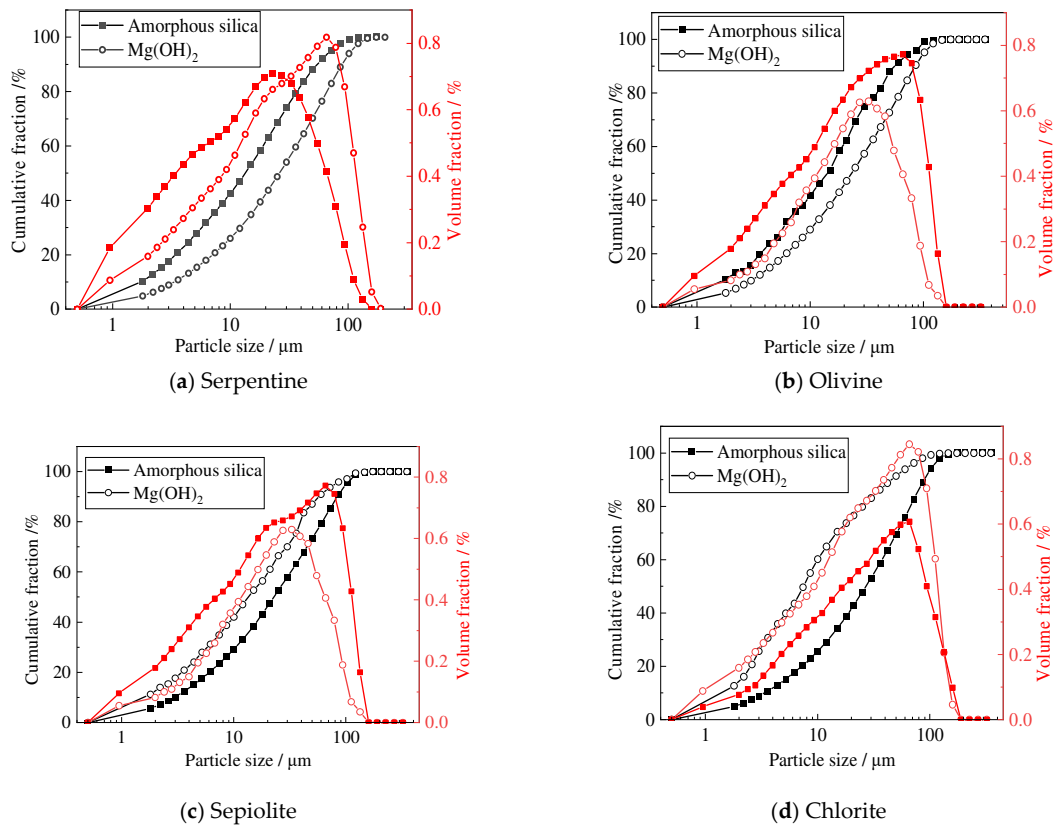


Figure 6. Particle size distribution of filter residue and Mg(OH)₂.

3.2. XRD and FTIR Analysis

Figures 7–10 are XRD patterns of the paste of the residue and MgO in 50 °C and 80 °C water. In the Figures 7–10, there is no distinct MgO diffraction peak, indicating that most of MgO has hydrated after 3 d. The characteristic peaks of M-S-H at the 2θ value of 5.0°–10.0°, 35.0°, and 59.9° can be observed [18,19] after 3 d. With the hydration time and the curing temperature, the height of these diffraction peaks gradually increases, while the corresponding $\text{Mg}(\text{OH})_2$ diffraction peaks decrease. The mineral diffraction peaks observed around 2θ at 35° in the samples prepared from chlorite may be attributed to minerals such as augite-Ca (PDF No. 24-0201) present in the chlorite raw materials.

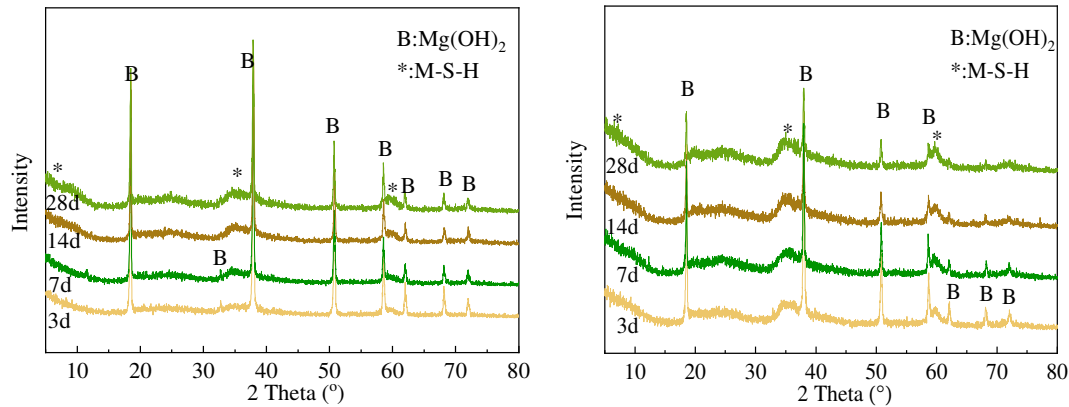


Figure 7. XRD of filter residue and MgO pastes of serpentine at 50 °C and 80 °C.

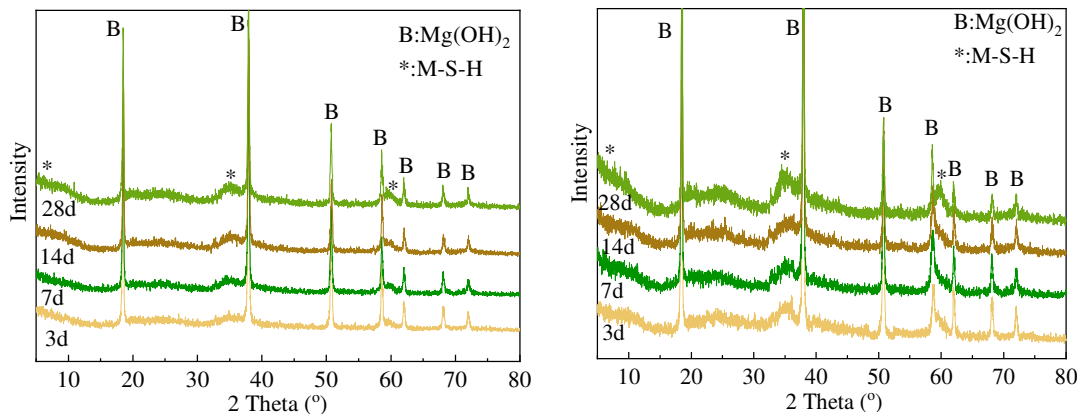


Figure 8. XRD of filter residue and MgO pastes of olivine at 50 °C and 80 °C.

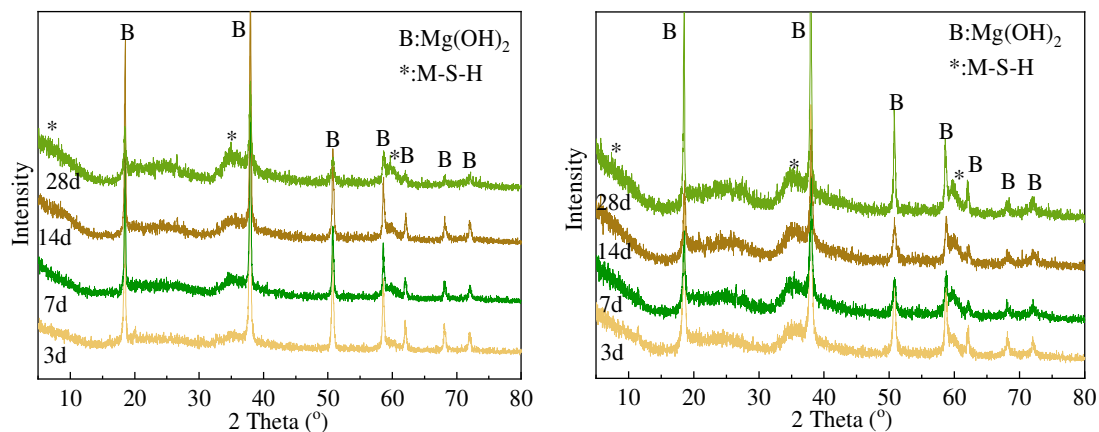


Figure 9. XRD of filter residue and MgO pastes of sepiolite at 50 °C and 80 °C.

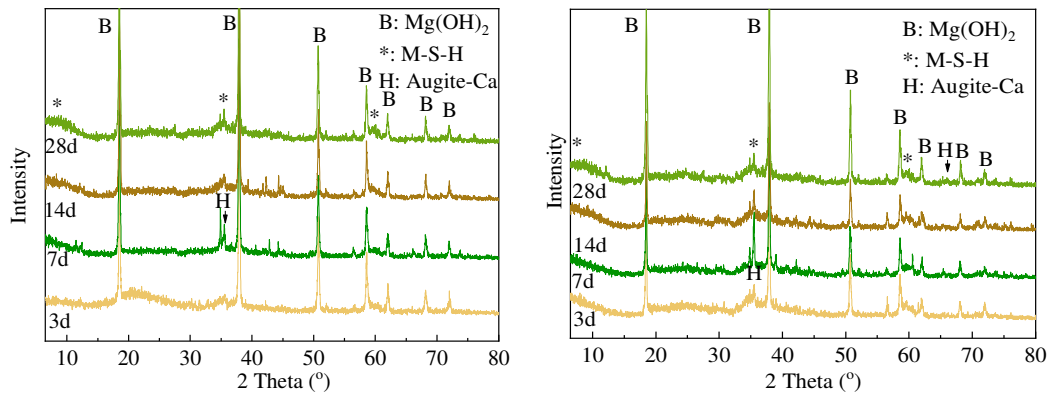


Figure 10. XRD of filter residue and MgO pastes of chlorite at 50 °C and 80 °C.

Figures 11–14 show the FTIR spectra of the residue and MgO paste at different reaction times under curing at 50 °C and 80 °C. The two absorption bands correspond to the formation of M-S-H. Specifically, the absorption band within the range of 950 to 1100 cm^{-1} is attributed to the Q^3 Si-O vibration, while the absorption band within the range of 870 to 920 cm^{-1} is attributed to the Q^2 Si-O vibration [5,19]. Additionally, the absorption peak observed near the wavenumber of 650 cm^{-1} can be attributed to the bending vibration of Si-O-Si [20]. With an increase in curing time, the intensities of these three absorption bands are significantly enhanced, indicating a gradual increase in the formation of hydration products. The absorption band at the wavenumber of 1080 cm^{-1} assigned the vibration of Si-O-Mg in M-S-H [7,21,22] also increases with age. These results are consistent with the XRD results.

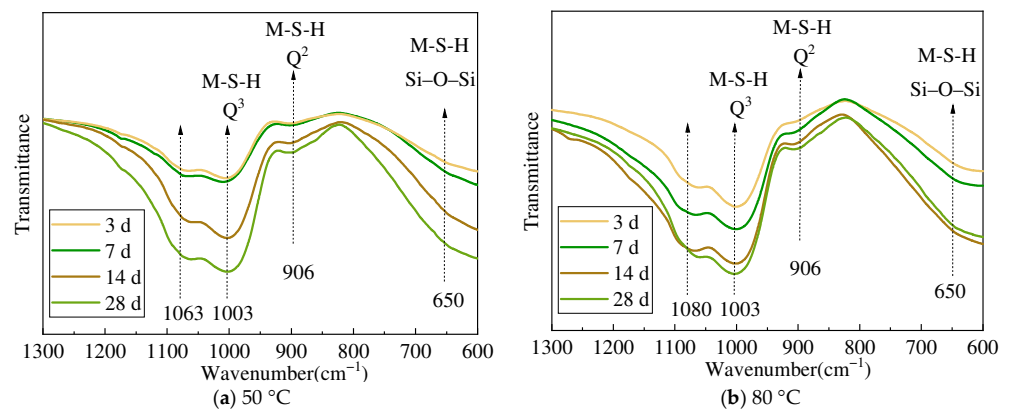


Figure 11. M-S-H FTIR spectra of serpentine cured at 50 °C and 80 °C.

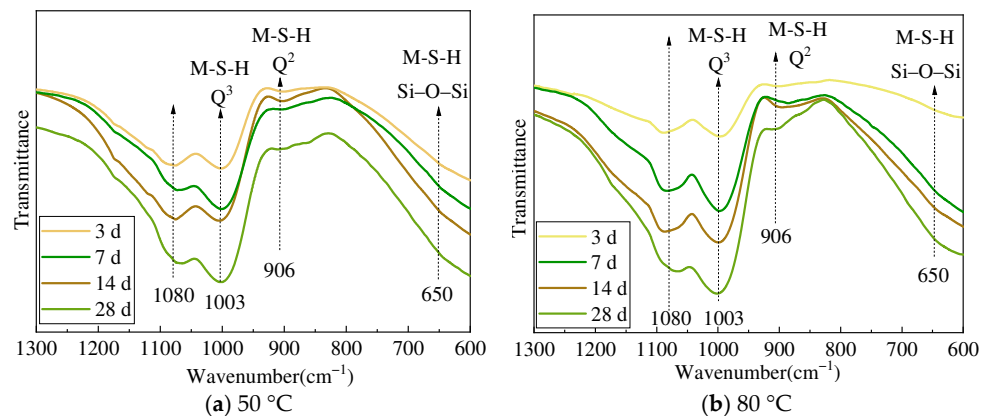


Figure 12. M-S-H FTIR spectra of olivine cured at 50 °C and 80 °C.

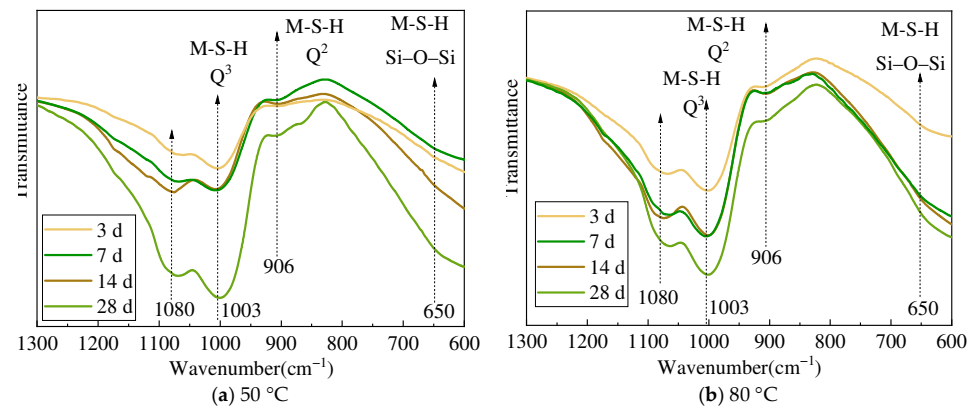


Figure 13. M-S-H FTIR spectra of sepiolite cured at 50 °C and 80 °C.

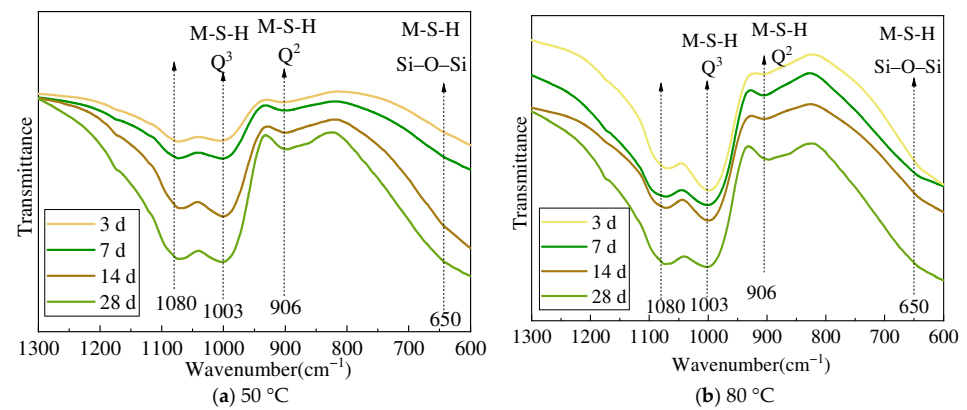


Figure 14. M-S-H FTIR spectra of chlorite cured at 50 °C and 80 °C.

3.3. TG and DSC Analysis

The mass loss between 50 °C and 300 °C (Δm_1) in the TG curve indicates the removal of interlayer water from M-S-H, and the weight loss between 300 °C and 750 °C (Δm_3) relates to the dehydroxylation of magnesium hydroxide and the decomposition of M-S-H (Figures 15–18, Table 3). Notably, this part of the mass loss includes the removal of the dehydroxylation of brucite at about 400 °C (Δm_2) [20,23]. With the increase in curing time, the water content between the layers of M-S-H gradually increases, reaching its maximum value at 7 days, followed by a decrease. The M-S-H phase itself acts as a gel-like material that can retain water within its structure; the continuous formation of it leads the increase in the interlayer water. But as the reaction progresses, the M-S-H phase becomes more densely packed, limiting the amount of water that can be accommodated in the interlayer spaces.

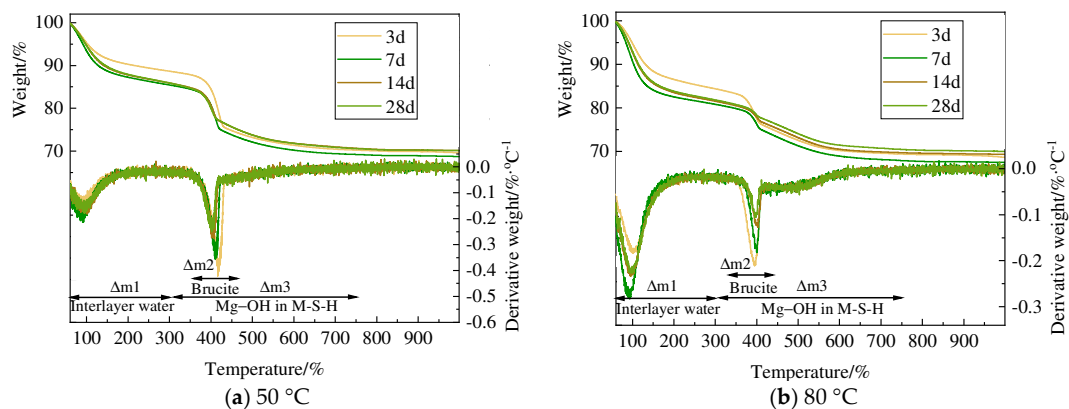


Figure 15. TG curve of serpentine of hydrated magnesium silicate.

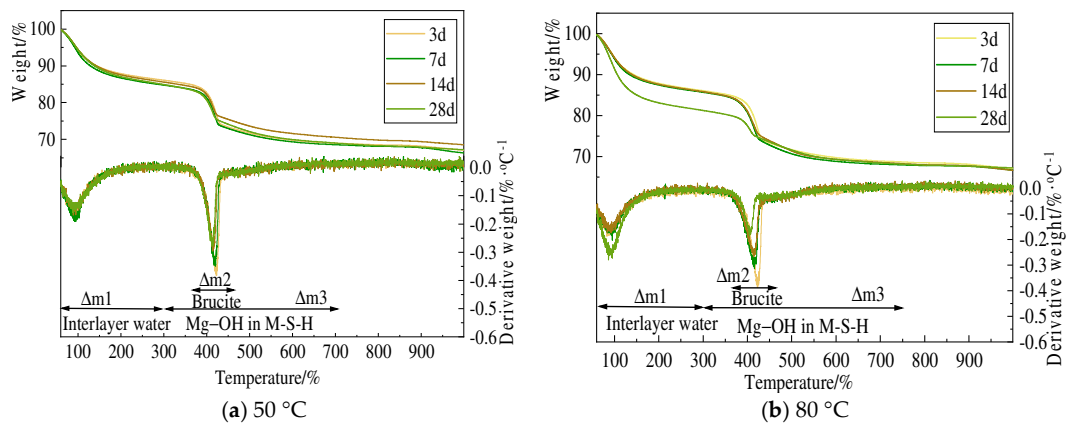


Figure 16. TG curve of olivine of hydrated magnesium silicate.

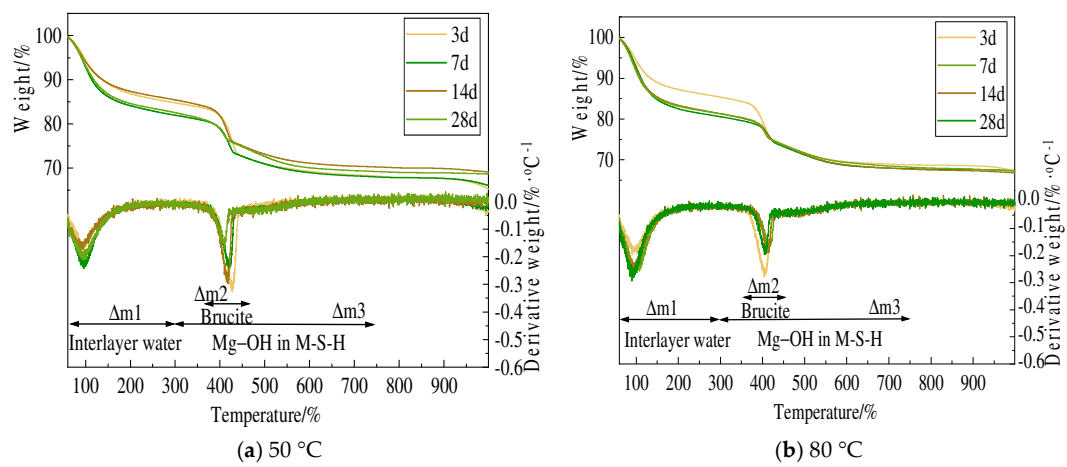


Figure 17. TG curve of sepiolite of hydrated magnesium silicate.

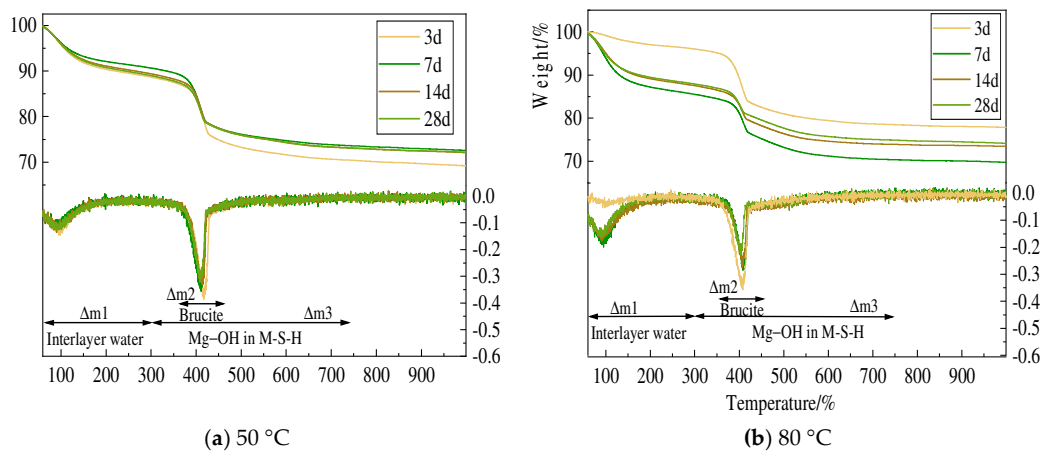


Figure 18. TG curve of chlorite of hydrated magnesium silicate.

Upon curing at 50 °C for 3 days, the mass loss due to Mg(OH)₂ dehydroxylation (Δm₂) reaches maximum value, gradually decreasing thereafter. Furthermore, at 28 days, the Mg(OH)₂ content is only about 70–80% of that of the four samples cured in 50 °C for 3 days. A higher-temperature curing accelerates the hydration reaction. For samples cured at 80 °C, this ratio decreases to 48–68%.

Table 3. The mass loss between different temperature wt%.

Curing Tem.	Mass Loss	Minerals	3 d	7 d	14 d	28 d
50 °C	Δm_1	Serpentine	11.34	14.55	14.07	14.07
		Olivine	13.92	15.25	14.43	15.09
		Sepiolite	15.21	18.02	14.56	17.43
		Chlorite	11.32	9.34	10.61	11.00
	Δm_2	Serpentine	13.07	10.70	9.16	9.02
		Olivine	11.75	10.72	8.87	9.33
		Sepiolite	11.41	8.28	9.10	6.02
		Chlorite	12.58	11.56	10.14	10.14
	Δm_3	Serpentine	18.44	16.25	15.28	15.35
		Olivine	17.36	16.44	15.43	16.32
		Sepiolite	16.61	13.97	15.18	13.32
		Chlorite	18.28	17.98	16.28	15.94
	$\Delta m_3 - \Delta m_2$	Serpentine	5.37	5.56	6.13	6.34
		Olivine	5.61	5.72	6.56	6.99
		Sepiolite	5.20	5.69	6.08	7.30
		Chlorite	5.70	6.42	6.14	5.80
80 °C	Δm_1	Serpentine	14.63	19.18	18.49	18.17
		Olivine	13.92	14.30	14.15	18.73
		Sepiolite	14.64	19.43	18.70	18.70
		Chlorite	14.48	12.46	12.09	13.99
	Δm_2	Serpentine	8.74	6.54	5.29	4.62
		Olivine	11.93	11.23	10.25	5.83
		Sepiolite	10.96	6.16	6.62	6.23
		Chlorite	8.60	7.60	6.60	5.89
	Δm_3	Serpentine	15.02	12.96	11.84	11.42
		Olivine	17.36	17.71	17.54	13.08
		Sepiolite	16.60	12.75	13.60	13.12
		Chlorite	15.13	13.60	13.00	12.50
$\Delta m_3 - \Delta m_2$	Serpentine	6.28	6.42	6.57	6.80	
	Olivine	5.43	6.48	7.29	7.25	
	Sepiolite	5.64	6.59	6.98	6.89	
	Chlorite	6.53	6.00	6.40	6.61	

Compared to the 3-day sample, the 28-day sample exhibited an increase in the mass loss ($\Delta m_3 - \Delta m_2$) of 118% to 140%. This means that the hydration rate decreased over time. A more compact structure, creating barriers for water transportation and decreasing the availability of reactants, hinders further hydration.

The DSC curves of M-S-H pastes prepared with serpentine, olivine, sepiolite, and chlorite are presented in Figures 19–22. On the DSC curve, the endothermic valley between 50 and 300 °C is caused by the removal of interlayer water from M-S-H. The second endothermic valley near 300–400 °C corresponds to the dehydroxylation of $Mg(OH)_2$. The heat release peak at about 850 °C is the heat release during the M-S-H recrystallization to form SiO_2 and enstatite ($MgSiO_3$) [6,24] or SiO_2 and Mg_2SiO_4 [25]. The heat release peak area of this region is calculated and illustrated in the figures. The heat release of the sample cured at 80 °C is greater than that of the sample cured at 50 °C; that is, the amount of M-S-H formed is higher at 80 °C. Furthermore, with the extension of the curing time, the heat release gradually increases, reaching its maximum at 14 days and slightly decreasing at 28 days (except for the sample prepared with olivine).

In Figures 19–22, an interesting observation can be made regarding the heat release peak at 850 °C. Initially, this peak exhibits a single peak or a double peak pattern at early age, but with extended curing time, it transitions into a single peak or a weakening of the double peaks (except for the sample prepared with olivine). This change is considered to be an indicative manifestation of M-S-H maturity [26].

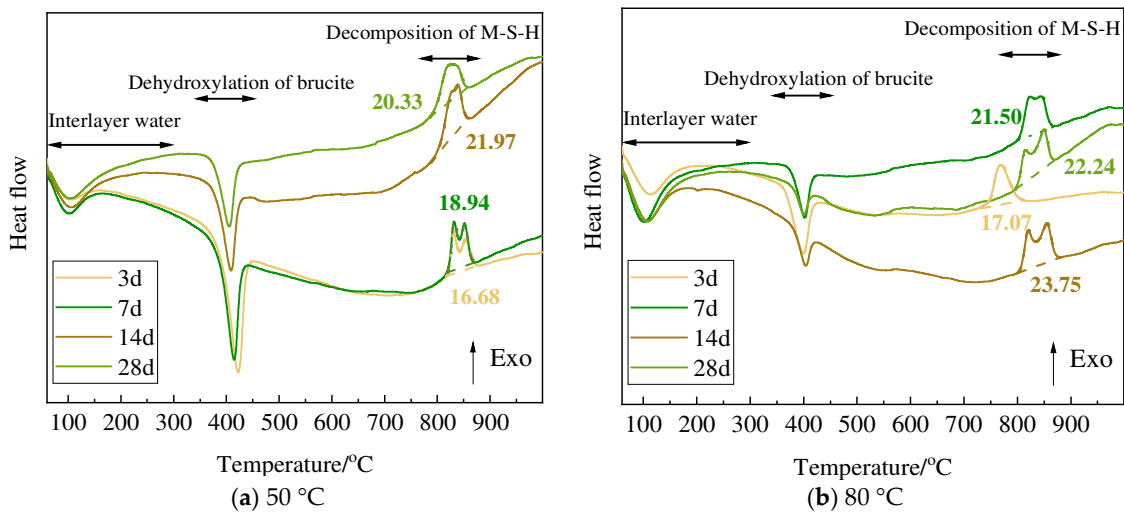


Figure 19. DSC curves of serpentine of M-S-H paste.

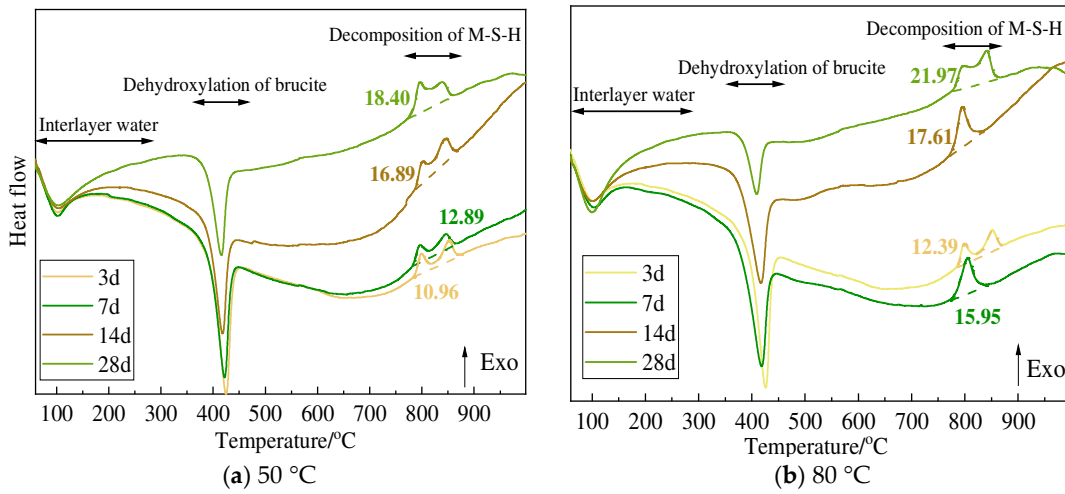


Figure 20. DSC curves of olivine of M-S-H paste.

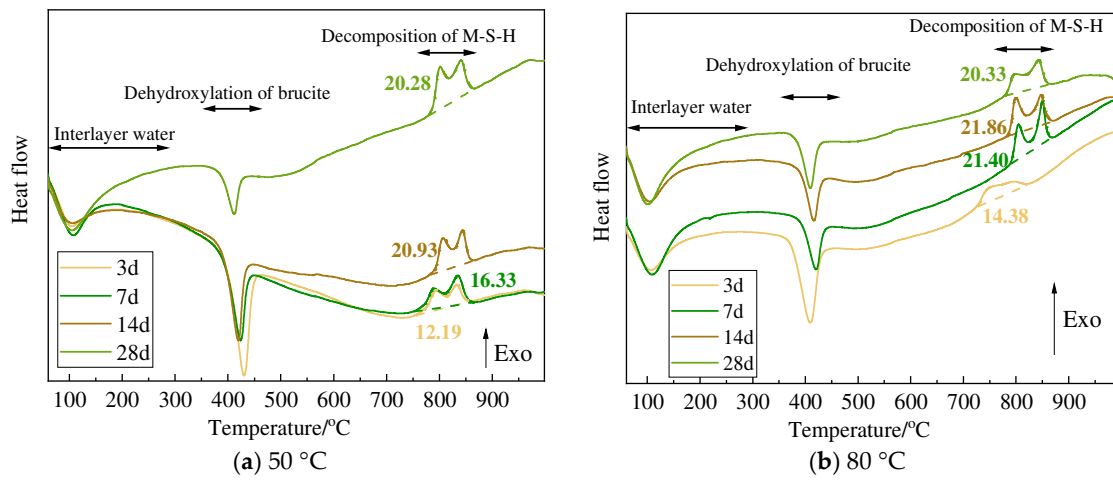


Figure 21. DSC curves of sepiolite of M-S-H paste.

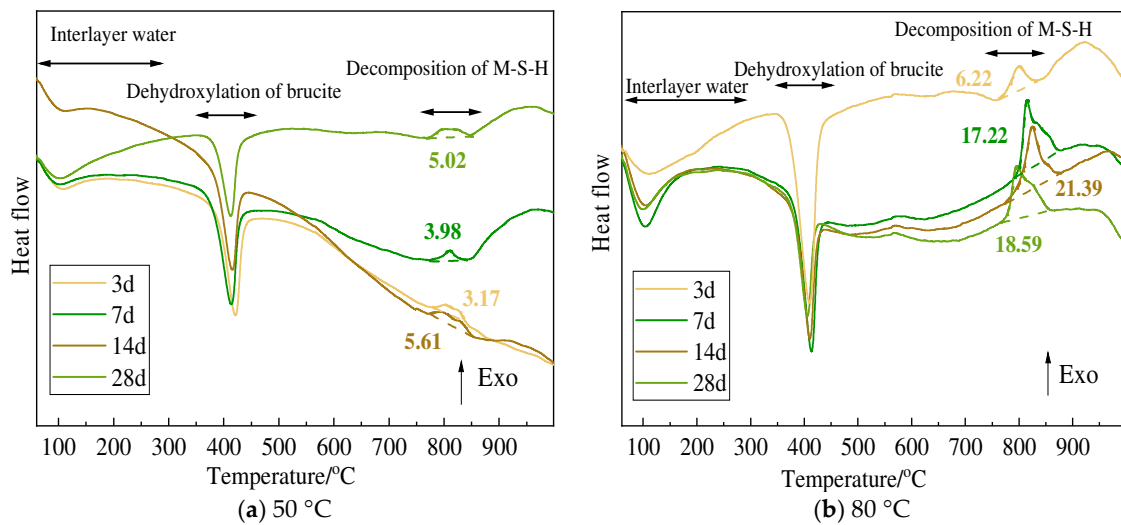


Figure 22. DSC curves of chlorite of M-S-H paste.

3.4. NMR Analysis

Figure 23 displays the ^{29}Si NMR spectra of the amorphous silica and M-S-H samples cured at 50 °C and 80 °C. The deconvolution results for these spectra at 28 d are summarized in Table 4. According to references [27–29], the chemical environment of ^{29}Si is denoted by Q^n , where n indicates the number of bridging oxygen atoms shared between a silicon tetrahedron and the surrounding silicon tetrahedra. In the spectrum of amorphous silica, the chemical shift at -112 cm^{-1} corresponds to the Q^4 signal, while -102 cm^{-1} represents the Q^3 signal [30]. The ^{29}Si MAS NMR spectra of amorphous silica obtained from the dissolution of four silicate minerals show no significant distinction for the aforementioned Q^3 and Q^4 signals. It is noted that the Q^4 signal in the M-S-H sample nearly vanishes after 28 days of curing. Furthermore, after 28 days of curing at 50 °C, the remaining Q^3 (-102 cm^{-1}) signal is slightly higher than that which underwent curing at 80 °C. From the relative content of the remaining Q^3 (-102 cm^{-1}) signal, a higher degree of hydration occurs at elevated curing temperatures. Due to the highest residual Q^3 content in amorphous silica, the M-S-H prepared from sepiolite has the lowest degree of hydration. Conversely, the M-S-H prepared using olivine as the raw material has the highest degree of hydration.

The ^{29}Si MAS NMR spectrum of M-S-H is primarily composed of chain end-group Q^1 , branched silicon–oxygen tetrahedron Q^2 , and layered silicon–oxygen tetrahedron Q^3 [28,31]. According to Bernard [3,32], the chemical shifts at $\sim -78.3\text{ ppm}$, -80 ppm , -85.5 ppm , -92.7 ppm , -94.7 ppm , and -96.7 ppm represent Q^1_a , Q^1_b , Q^2 , Q^3_a , Q^3_b , and Q^3_c , respectively. The relative content of Q^1 in the samples cured at 80 °C is lower compared to that in the samples cured at 50 °C, indicating that high-temperature curing enhances the polymerization of silicate tetrahedra in M-S-H. As can be seen from the spectral peak shapes and Table 4, the formation rate of the Q^3 structure in M-S-H prepared with serpentine, olivine, and sepiolite exceeds that of the Q^2 structure within the first 28 days. Unlike these three minerals, the M-S-H prepared from chlorite has a higher relative content of Q^2 than of Q^3 . This indicates that the M-S-H prepared from chlorite has the lowest degree of polymerization of silicate tetrahedra. In all samples, the relative amount of Q^3_b , which represents the talc-like T:O:T structure with a chemical shift at -94.7 ppm , is lower than that of Q^3_a , which represents the chrysotile-like T:O structure. This indicates that the silicate tetrahedral structure of the M-S-H prepared using these four silicates is closer to the chrysotile-like T:O structure.

Owing to the characteristic layered structure of the M-S-H samples, the M-S-H derived from sepiolite demonstrated a greater relative Q^3/Q^2 concentration compared to the M-S-H derived from other sources. This indicates a higher degree of tetrahedral polymerization when sepiolite is used as the raw material. Compared to other minerals, sepiolite has the

highest content of residual unreacted silica, resulting in the highest Mg/Si ratio in the system. A higher Mg/Si ratio leads to an increase in the Q^3/Q^2 of the produced M-S-H.

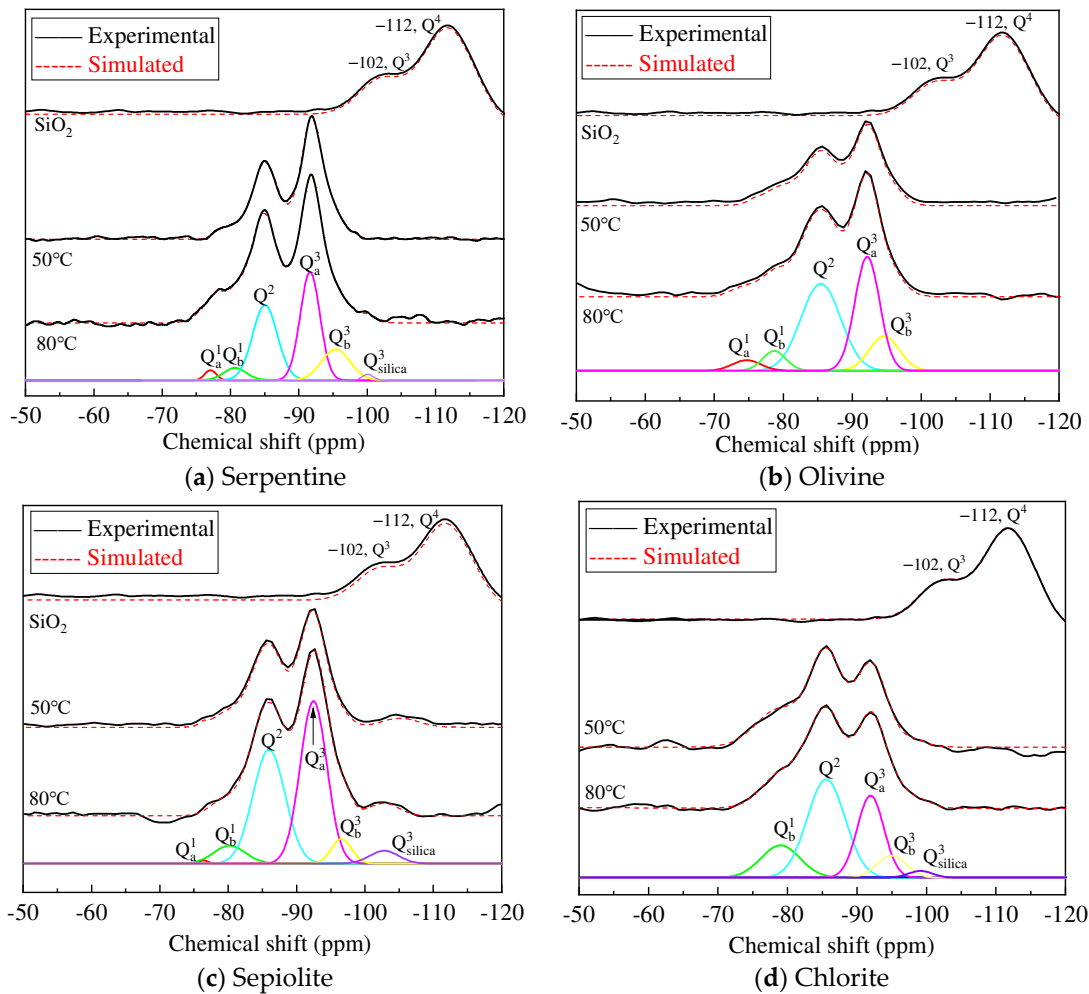


Figure 23. Deconvolution demonstration of ^{29}Si SSNMR spectra for MSH pastes at 28 d.

Table 4. Relative concentrations of different silicon sites of MSH pastes obtained from deconvolution demonstration of ^{29}Si SSNMR spectra.

Curing Tem.	Minerals	I/%					Unreacted Silica I/%		Q^3/Q^2
		Q^1_a	Q^1_b	Q^2	Q^3_a	Q^3_b	Q^3	Q^4	
SiO ₂	Serpentine						31.4	68.6	
	Olivine						31.8	68.2	
	Sepiolite						30.9	69.1	
	Chlorite						32.4	67.6	
50 °C	Serpentine	4.6	7.8	41.1	32.6	10.1	3.8		1.04
	Olivine	5.8	7.3	43.8	35.6	7.5	0		0.98
	Sepiolite	1.2	4.2	36.1	43.7	5.1	9.7		1.35
	Chlorite	0	23.8	40.7	18.9	14.7	1.9		0.83
80 °C	Serpentine	4.3	7.1	43.6	35.9	7.9	1.2		1.00
	Olivine	4.1	6.1	46.4	37.1	6.3	0		0.94
	Sepiolite	0.7	5.4	38.9	45.9	5.2	3.9		1.31
	Chlorite	0	24.4	43.4	20.2	11.6	0.4		0.73

3.5. Compressive Strength Analysis

The compressive strength of hydrated magnesium silicate paste is shown in Figure 24. The figure clearly demonstrates that the compressive strength of M-S-H gradually increases with the curing time, surpassing 38 MPa at 28 days. The M-S-H specimens cured at 80 °C exhibit higher strength compared to those cured at 50 °C. However, the strength ratio of specimens cured at 80 °C to those at 50 °C gradually decreases, indicating that curing temperature has a more significant impact on the early compressive strength of the specimens. With an increase in curing time, the strength difference caused by environmental temperature gradually diminishes.

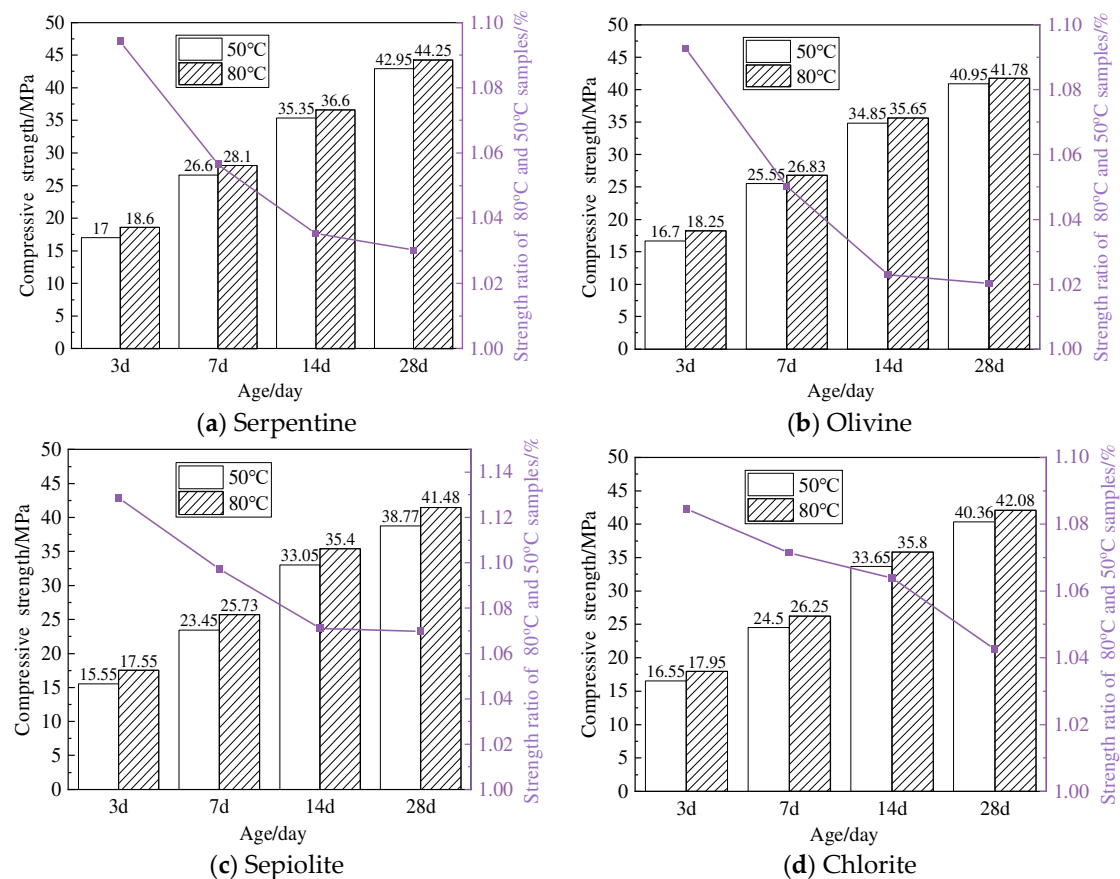


Figure 24. Compressive strength of M-S-H cured at different temperatures at 3 d, 7 d, 14 d, and 28 d.

Analyzing the relationship between compressive strength and mass loss at different temperature ranges in Figure 25, it is observed that the mass loss (Δm_1) between 50 °C and 300 °C shows the weakest correlation with strength. This is because the water evaporated during this temperature range includes not only interlayer water from M-S-H but also a certain amount of free water or adsorbed water. On the other hand, the removal of hydroxyl groups (Δm_2) from brucite, which acts as a reactant in M-S-H formation, exhibits a strong negative correlation with M-S-H strength. Subtracting the mass loss of brucite at approximately 400 °C (Δm_2) from the mass loss between 300 °C and 750 °C (Δm_3) provides the remaining mass loss, which represents the decomposition of M-S-H. The mass loss demonstrates the strongest correlation with strength.

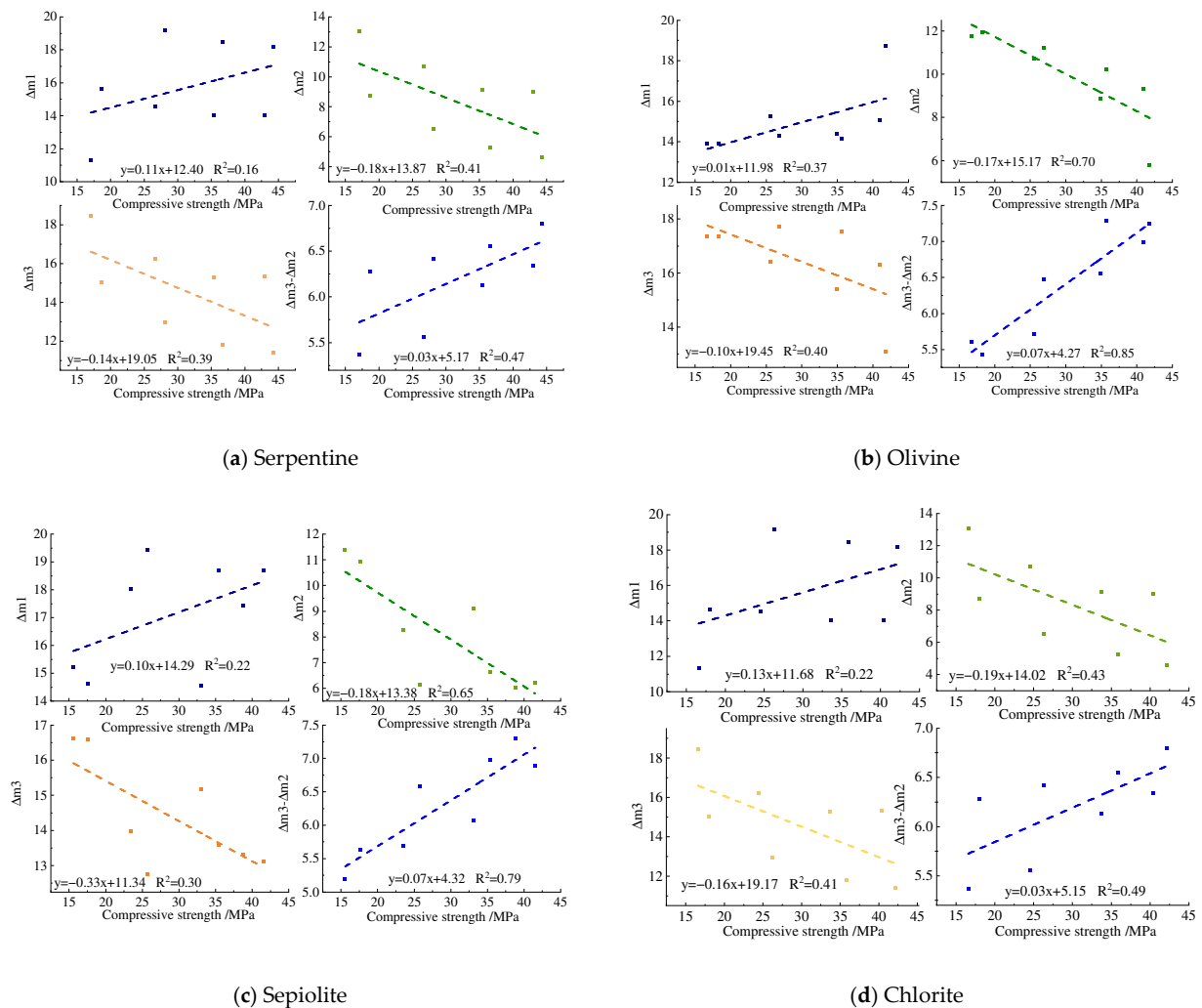


Figure 25. The relationship between the strength and mass loss at different temperature ranges.

4. Conclusions

In this study, four types of natural magnesium silicate minerals were used as raw materials. Through the acid-leaching method, high-purity amorphous silica and magnesium hydroxide were obtained. Using these intermediates, magnesium silicate hydrate cementitious materials were prepared. The main conclusions drawn are as follows:

- (1) The amorphous silica obtained from the acid leaching of serpentine, olivine, sepiolite, and chlorite reach a purity of over 90%. The silica derived from serpentine, olivine, and sepiolite has an average particle size of about 20 μm , while the silica from acid-leached chlorite has an average particle size of about 65 μm .
- (2) Amorphous silica and magnesium oxide prepared using magnesium hydroxide could form magnesium silicate hydrate within 3 days of hydration. Although there are certain numerical differences between the minerals used as raw materials, in general, the hydration reaction accelerates by 10–20% with increased curing time and temperature, and the degree of polymerization of the silicate tetrahedra of newly formed M-S-H increases.
- (3) The M-S-H prepared using four types of magnesium silicate minerals forms a silicate tetrahedral structure predominantly characterized by the chrysotile-like T:O structure. The resulting magnesium silicate hydrate cementitious materials could achieve a compressive strength of 40 MPa at 28 days, and the compressive strength shows a good correlation with the reduction in magnesium hydroxide content and the increase in magnesium silicate hydrate.

Author Contributions: Conceptualization, Q.S. and Y.C.; Methodology, Q.S. and Y.C.; Software, Q.H.; Formal analysis, F.C.; Investigation, Q.S., J.N., T.S. and Y.H.; Resources, T.S., Y.H. and Y.D.; Data curation, Q.H., J.N., T.S., Y.H. and Y.D.; Writing—original draft, Q.H.; Writing—review & editing, Q.S.; Visualization, J.N., H.Z. and F.C.; Supervision, H.Z.; Project administration, Y.C. and F.C.; Funding acquisition, H.Z., Y.C. and Y.D. All authors have read and agreed to the published version of the manuscript.

Funding: This work was supported by the Research and Development Plan of Shaanxi Province of China (2022KXJ-008, 2022GY-418, 2023GXLH-05, 22023JBGS-19), the Key Scientific Research Projects of Shaanxi Provincial Department of Education of China (20JS079, 20JY040), and the Shaanxi Science and Technology Innovation Team (2021TD-53).

Data Availability Statement: Data are contained within the article.

Conflicts of Interest: Hong Zhou was employed by the company Shaanxi Building Materials Technology Group Co., Ltd.; Yang Deng was employed by the company Shaanxi Fuping Eco-Cement Co., Ltd. The remaining authors declare that the research was conducted in the absence of any commercial or financial relationships that could be construed as a potential conflict of interest.

References

1. Gartner, E.; Sui, T. Alternative cement clinkers. *Cem. Concr. Res.* **2018**, *114*, 27–39. [[CrossRef](#)]
2. Simoni, M.; Woo, C.L.; Zhao, H.; Iuga, D.; Svora, P.; Hanein, T.; Kinoshita, H.; Walkley, B. Reaction mechanisms, kinetics, and nanostructural evolution of magnesium silicate hydrate (M-S-H) gels. *Cem. Concr. Res.* **2023**, *174*, 107295. [[CrossRef](#)]
3. Bernard, E.; Lothenbach, B.; Le Goff, F.; Pochard, I.; Dauzères, A. Effect of magnesium on calcium silicate hydrate (C-S-H). *Cem. Concr. Res.* **2017**, *97*, 61–72. [[CrossRef](#)]
4. Bernard, E.; Lothenbach, B.; Rentsch, D.; Pochard, I.; Dauzères, A. Formation of magnesium silicate hydrates (M-S-H). *Phys. Chem. Earth* **2017**, *99*, 142–157. [[CrossRef](#)]
5. Nied, D.; Enemark-Rasmussen, K.; L'Hopital, E.; Skibsted, J.; Lothenbach, B. Properties of magnesium silicate hydrates (MSH). *Cem. Concr. Res.* **2016**, *79*, 323–332. [[CrossRef](#)]
6. Zhang, T.; Cheeseman, C.; Vandeperre, L. Development of low pH cement systems forming magnesium silicate hydrate (MSH). *Cem. Concr. Res.* **2011**, *41*, 439–442. [[CrossRef](#)]
7. Sonat, C.; Unluer, C. Development of magnesium-silicate-hydrate (M-S-H) cement with rice husk ash. *J. Clean. Prod.* **2019**, *211*, 787–803. [[CrossRef](#)]
8. Du, Y. Preparation of Magnesium-Silicate-Hydrate Cement by Replacing Silica Fume with Pulverized Fuel Ash. Ph.D. Thesis, Dalian University of Technology, Dalian, China, 2016.
9. Chen, S.; Wang, L. Mechanical properties and reaction products of reactive MgO modified circulating fluidized bed combustion slag-silica fume composites. *Acta Mater. Compos. Sin.* **2018**, *35*, 1288–1297.
10. Abdel-Gawwad, H.A.; El-Aleem, S.A.; Amer, A.A.; El-Didamony, H.; Arif, M.A. Combined impact of silicate-amorphicity and MgO-reactivity on the performance of Mg-silicate cement. *Construct. Build. Mater.* **2018**, *189*, 78–85. [[CrossRef](#)]
11. Du, Y.C.; Wang, X.K.; Wu, J.S.; Wang, J.S.; Li, Y.; Dai, H.X. Mg₃Si₄O₁₀(OH)₂ and MgFe₂O₄ in situ grown on diatomite: Highly efficient adsorbents for the removal of Cr(VI). *Micropor. Mesopor. Mat.* **2018**, *271*, 83–91. [[CrossRef](#)]
12. Temuujin, J.; Okada, K.; Mackenzie, K.J.D. Formation of layered magnesium silicate during the aging of magnesium hydroxide-silica mixtures. *J. Am. Ceram. Soc.* **2010**, *81*, 754–759. [[CrossRef](#)]
13. Wedepohl, K.H. The composition of the continental crust. *Miner. Mag.* **1994**, *58*, 1217–1232. [[CrossRef](#)]
14. Rüter, D.; Austrheim, H. Formation of magnesium silicate hydrate cement in nature. *J. Geol. Soc.* **2018**, *175*, 308–320. [[CrossRef](#)]
15. Lu, Z.; Wan, P.; Su, G.; Li, H. A Study of the cementitious behaviour of dehydrating serpentine in hydrothermal condition. *J. Chin. Ceram. Soc.* **1997**, *25*, 384–388. (In Chinese)
16. Bernard, E.; Lothenbach, B.; Cau-Dit-Coumes, C.; Pochard, I.; Rentsch, D. Aluminum incorporation into magnesium silicate hydrate (M-S-H). *Cem. Concr. Res.* **2020**, *128*, 105931. [[CrossRef](#)]
17. GB/T 17671-1999; Method of Testing Cements—Determination of Strength. State Administration of Quality and Technical Supervision of China: Beijing, China, 1999.
18. Li, Z.; Yu, Q.; Chen, X.; Liu, H.; Zhang, J.; Zhang, J.; Yang, Y.; Wei, J. The role of MgO in the thermal behavior of MgO-silica fume pastes. *J. Therm. Anal. Calorim.* **2017**, *127*, 1897–1909. [[CrossRef](#)]
19. Brew, D.R.M.; Glasser, F.P. Synthesis and characterisation of magnesium silicate hydrate gels. *Cem. Concr. Res.* **2005**, *35*, 85–98. [[CrossRef](#)]
20. Lothenbach, B.; Nied, D.; L'Hôpital, E.; Achiedo, G.; Dauzères, A. Magnesium and calcium silicate hydrates. *Cem. Concr. Res.* **2015**, *77*, 60–68. [[CrossRef](#)]
21. Zhang, T.; Zou, J.; Wang, B.; Wu, Z.; Jia, Y.; Cheeseman, C.R. Characterization of magnesium silicate hydrate (MSH) gel formed by reacting MgO and Silicafume. *Materials* **2018**, *11*, 909. [[CrossRef](#)]

22. Zhang, T.; Li, T.; Zou, J.; Li, Y.; Zhi, S.; Jia, Y.; Cheeseman, C.R. Immobilization of radionuclide ^{137}Cs by magnesium silicate hydrate cement. *Materials* **2019**, *13*, 146. [[CrossRef](#)]
23. Zhang, S.; Liao, N.; Li, Y.; Chatterjee, A.; Zhang, Y.; Sang, S. M-S-H formation in MgO-SiO_2 slurries via wet milling for magnesia based castables. *Ceram. Int.* **2021**, *47*, 10880–10886. [[CrossRef](#)]
24. Chabrol, K.; Gressier, M.; Pebere, N.; Menu, M.-J.; Martin, F.; Bonino, J.-P.; Marichal, C.; Brendle, J. Functionalization of synthetic talc-like phyllosilicates by alkoxyorganosilane grafting. *J. Mater. Chem.* **2010**, *20*, 9695–9706. [[CrossRef](#)]
25. Park, D.G.; Duchamp, J.C.; Duncan, T.M.; Burlitch, J.M. Preparation of forsterite by pyrolysis of a xerogel: The effect of water. *Chem. Mater.* **1994**, *6*, 1990–1995. [[CrossRef](#)]
26. Walling, S.A.; Kinoshita, H.; Bernal, S.A.; Collier, N.C.; Provis, J.L. Structure and properties of binder gels formed in the system $\text{Mg}(\text{OH})_2\text{-SiO}_2\text{-H}_2\text{O}$ for immobilisation of Magnox sludge. *Dalton Trans.* **2015**, *44*, 8126–8137. [[CrossRef](#)]
27. Roosz, C.; Grangeon, S.; Blanc, P.; Montouillout, V.; Lothenbach, B.; Henocq, P.; Giffaut, E.; Vieillard, P.; Gaboreau, S. Crystal structure of magnesium silicate hydrates (M-S-H): The relation with 2:1 Mg-Si phyllosilicates. *Cem. Concr. Res.* **2015**, *73*, 228–237. [[CrossRef](#)]
28. Martini, F.; Tonelli, M.; Geppi, M.; Ridi, F.; Borsacchi, S.; Calucci, L. Hydration of MgO/SiO_2 and Portland cement mixtures: A structural investigation of the hydrated phases by means of X-ray diffraction and solid state NMR spectroscopy. *Cem. Concr. Res.* **2017**, *102*, 60–67. [[CrossRef](#)]
29. Tonelli, M.; Martini, F.; Calucci, L.; Fratini, E.; Geppi, M.; Ridi, F.; Borsacchi, S.; Baglioni, P. Structural characterization of magnesium silicate hydrate: Towards the design of eco-sustainable cements. *Dalton Trans.* **2016**, *45*, 3294–3304. [[CrossRef](#)]
30. Ma, Y.; Li, W.; Jin, M.; Liu, J.; Zhang, J.; Huang, J.; Lu, C.; Zeng, H.; Wang, J.; Zhao, H.; et al. Influences of leaching on the composition, structure and morphology of calcium silicate hydrate (C-S-H) with different Ca/Si ratios. *J. Build. Eng.* **2022**, *58*, 105017. [[CrossRef](#)]
31. Masse, S.; Zanni, H.; Lecourtier, J.; Roussel, J.; Rivereau, A. ^{29}Si solid state NMR study of tricalcium silicate and cement hydration at high temperature. *Cem. Concr. Res.* **1993**, *23*, 1169–1177. [[CrossRef](#)]
32. Bernard, E.; Lothenbach, B.; Chlique, C.; Wyrzykowski, M.; Dauzères, A.; Pochard, I.; Cau-Dit-Coumes, C. Characterization of magnesium silicate hydrate (M-S-H). *Cem. Concr. Res.* **2019**, *116*, 309–330. [[CrossRef](#)]

Disclaimer/Publisher’s Note: The statements, opinions and data contained in all publications are solely those of the individual author(s) and contributor(s) and not of MDPI and/or the editor(s). MDPI and/or the editor(s) disclaim responsibility for any injury to people or property resulting from any ideas, methods, instructions or products referred to in the content.